Applied Catalysis B: Environmental 200 (2017) 141–149

Contents lists available at ScienceDirect

Applied Catalysis B: Environmental

journal homepage: www.elsevier.com/locate/apcatb

Co-porphyrin/carbon nitride hybrids for improved photocatalytic CO_2 reduction under visible light

Guixia Zhao[a], Hong Pang[a,b], Guigao Liu[a,b], Peng Li[a], Huimin Liu[a], Huabin Zhang[a], Li Shi[a,b], Jinhua Ye[a,b,c,d,*]

[a] International Center for Materials Nanoarchitectonics (WPI-MANA), National Institute for Materials Science (NIMS), 1-1 Namiki, Tsukuba, Ibaraki 305-0044, Japan
[b] Graduate School of Chemical Science and Engineering, Hokkaido University, Sapporo 060-0814, Japan
[c] TU-NIMS Joint Research Center, School of Materials Science and Engineering, Tianjin University, Tianjin 300072, PR China
[d] Collaborative Innovation Center of Chemical Science and Engineering, Tianjin 300072, PR China

ARTICLE INFO

Article history:
Received 27 May 2016
Received in revised form 24 June 2016
Accepted 29 June 2016
Available online 30 June 2016

Keywords:
Photocatalysis
CO_2 reduction
Carbon nitride
Co-porphyrin
Covalent hybrids

ABSTRACT

A covalently linked reaction center/antenna hybrid composed of Co-porphyrin and low-molecular-weight carbon nitride was developed for the reduction of CO_2 into CO under visible light for the first time. The hybrids possessed thirteen-fold higher photocatalytic activity (17 μmol/g/h) compared with bulk carbon nitride, and it is more than twice what it was in the Co-porphyrin loaded C_3N_4 heterojunction system. The efficient electron transfer and trapping by the Co active sites as well as the affinity of Co-porphyrin for CO_2 are considered to account for the enhanced activity. Our findings may open a promising route to modify carbon nitride and provide a feasible approach to immobilize the active site into the light-harvest antenna for efficient electron-hole separation, electron transferring and the following redox reaction in photocatalytic process, which reforms the conventional semiconductor-cocatalyst heterojunction system.

1. Introduction

Due to the contemporary energy shortage, CO_2 conversion into chemical fuels through artificial photosynthesis has attracted much interest due to the massively available CO_2 from industrial release. Although plenty of research has been focused on exploring efficient photocatalysts and co-catalysts for CO_2 reduction [1–8], the performance is still far from satisfied due to the difficulties in combining the suitable semiconductor with visible light response and the matched co-catalyst, especially controlling of electron transferring between them, as well as the CO_2 affinity on to the active sites [9].

Graphitic carbon nitride (melon) is believed to be a promising semiconductor for CO_2 reduction owning to its high conduction band [10]. Much research has been focused on the CO_2 photoreduction with pure C_3N_4 [11] or C_3N_4-based heterostructure [12–17]. For a typical example, combining with the efficiency and selectivity of supramolecular complex, Kuriki et al. has successfully used a ruthenium complex as the catalytic units for the reduction of CO_2 into formic acid with C_3N_4 as light-harvest units [18]. Considering the complicated preparation process of ruthenium complex and the rarity of Ru, non-noble metal based molecule catalyst should be a better choice for more economically viable application. In the past year, molecule catalysts have been widely studied for electrochemical CO_2 reduction. For instance, Covalent organic frameworks containing cobalt porphyrin, Co(II) complex and Fe(III) complex with pentadentate N5 ligand were proved to be promising for efficient CO_2 reduction [19,20]. Shen et al. also confirmed highly CO_2 reduction performance by immobilizing Co-based porphyrins onto pyrolytic graphite electrode [21]. Similarly, a pyrene-appended iron triphenyl porphyrin immobilized on carbon nanotubes via noncovalent interactions showed highly selective and rapid catalytic activity for the CO_2 reduction in water [22].

Considering the more convenient powder photocatalytic system without the expensive transparent electrodes and the directional illumination, it is really worth considering how to combine the star semiconductor (i.e., graphitic carbon nitride) with these active molecule catalysts (i.e., Co-porphyrin) for photocatalytic CO_2 fixation. Inspired by the sophisticated structure in the plant photosynthetic system, it is hopeful to enhance the CO_2 reduction by

* Corresponding author at: International Center for Materials Nanoarchitectonics (WPI-MANA), National Institute for Materials Science (NIMS), 1-1 Namiki, Tsukuba, Ibaraki 305-0044, Japan.
E-mail address: Jinhua.YE@nims.go.jp (J. Ye).

http://dx.doi.org/10.1016/j.apcatb.2016.06.074
0926-3373/

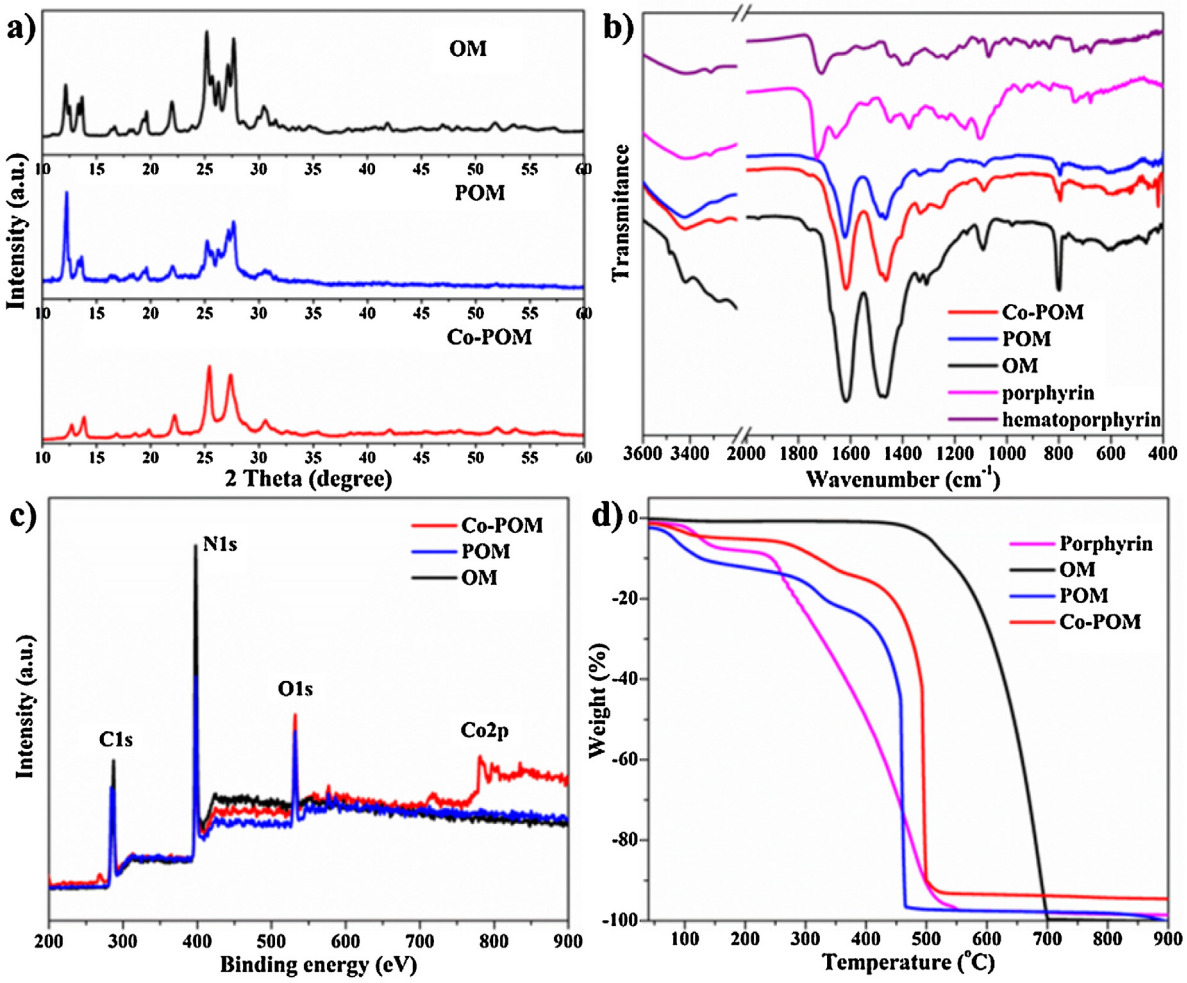

Fig. 1. (a) XRD patterns and (c) XPS of OM, POM and Co-POM; (b) FTIR spectrum of hematoporphyrin, porphyrin, OM, POM and Co-POM; (d) TGA trace for porphyrin, OM, POM and Co-POM.

some efficient linkage between the semiconductor and molecule catalyst. Bearing these in mind, we have constructed reaction center/antenna hybrids, i.e., Co-porphyrin covalently immobilized with oligomers of melems through Schiff base chemistry between the oligomer of melem and porphyrin and further metallization of the porphyrin-site. As expected, the band structure of this architecture can be reformatted from these two sub-units and improved CO_2 reduction can be realized on the metal-porphyrin site by utilizing the irradiated electron from the new C-N framework.

Scheme S1 (Supplementary Information) shows the formation of the porphyrin-oligomers of melems (POM) hybrid and Co-porphyrin-oligomers of melems (Co-POM). Oligomers of melems (OM) were synthesized by heat treatment of melamine at 450 °C. Porphyrin (P) was oxidized from hematoporphyrin by Jone's reagent. Covalent hybrid POM was obtained through the condensation between amino-group from OM and ketonic-group from porphyrin. Co-POM was finally formed after refluxing POM and $CoCl_2$ mixture in DMF.

2. Experimental

2.1. Material preparation

The oligomers of melems (OM) were prepared by heating melamine in a covered crucible in a muffle furnace in air at 8 K min^{-1} to 450 °C, holding at this temperature for 4 h and cooled down to room temperature at 4 K min^{-1}. The resulted product is noted as OM. For OM(430) and OM(480), the preparation is similar to OM except that the calcination temperature is 430 °C and 480 °C, respectively. Melon prepared at 550 °C is also used for the following section.

Hematoporphyrin was oxidized by Jone's reagent. Firstly, Jone's reagent was prepared by dissolving 2.672 g of CrO_3 in 2.3 mL of concentrated sulphuric acid and diluting with water to 10 mL. Then, 100 mg of hematoporphyrin was dissolved in 60 mL of acetone. 0.1 mL of Jone's reagent was added into the solution within 15 min. After stirring for 30 min, 15 mL of isopropanol was added to quench the excessive Jone's reagent. After removing the solvent, the oxidized hematoporphyrin was separated by silica gel column, and the resulted product is noted as porphyrin. For Ketone-Ammonia condensation was catalyzed by acetic acid in anhydrous ethanol with anhydrous $MgSO_4$ as dehydrating agent. Typically, 200 mg of OM, 200 mg of porphyrin and 50 mg of anhydrous $MgSO_4$ were mixed in 100 mL of anhydrous ethanol. Drops of acetic acid were added before refluxing at 80 °C for 48 h. After centrifugation and washing, the resulted POM was dried in vacuum-oven at 30 °C. For POM(0.6) and POM(1.1), similar synthesis was carried except the amount of porphyrin is changed into 120 mg and 220 mg, respectively. POM(430) and POM(480) were prepared in a similar approach by using OM(430) and OM(480) instead of OM.

Metallization of POM to form Co-POM can be realized by refluxing POM with $CoCl_2$ in DMF at 100 °C for 24 h. The resulted products

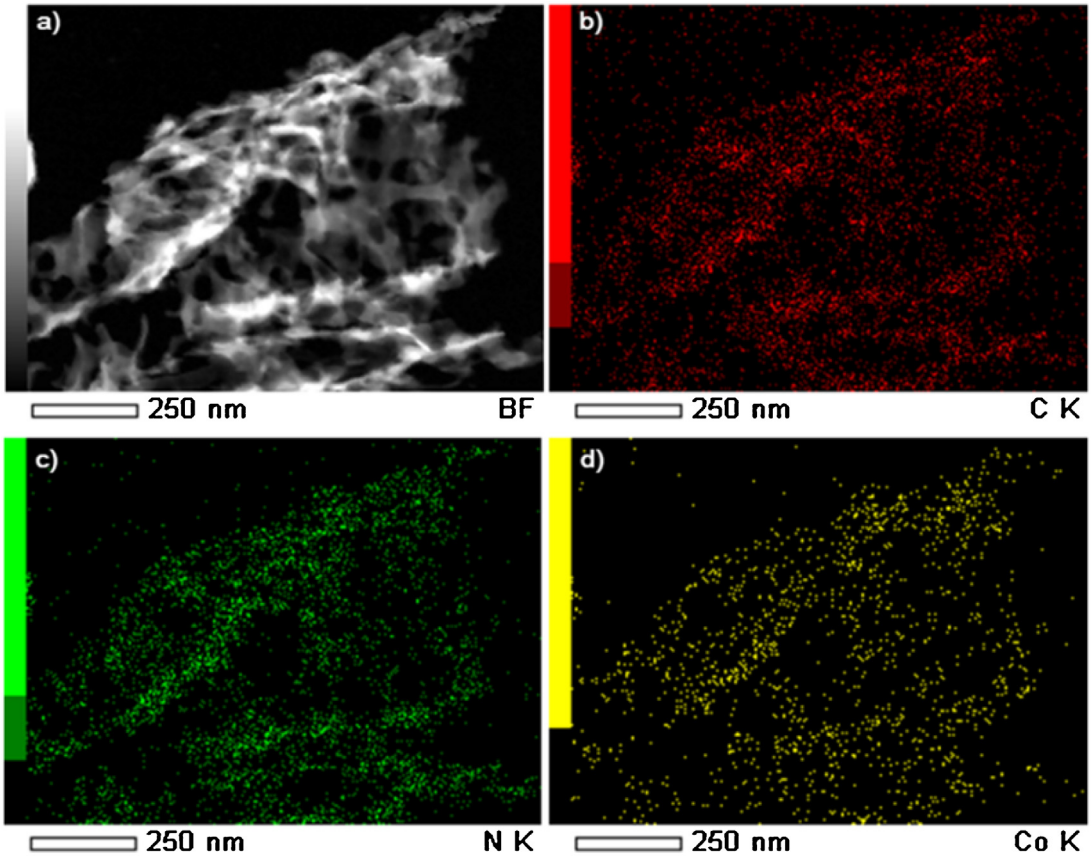

Fig. 2. (a) TEM image of Co-POM; (b–d) the corresponding EDS mapping images of Carbon, Nitrogen and Cobalt elements.

were washed with deionized water and dried at 30 °C overnight. The same process is applied for POM(0.6), POM(430) and POM(480) to form Co-POM(0.6), Co-POM(430) and Co-POM(480), respectively. The metallization is also carried out for porphyrin to form Co-P, which is separated by silica gel column.

Melon was prepared by heating melamine 8 K min^{-1} to 550 °C, holding at this temperature for 4 h, and cooled to RT at 4 K min^{-1}. Melon and Co-P in different ratio in ethanol solution was stirred for 12 h at 40 °C and after evaporating the solvent, the mixture was dried in oven at 30 °C overnight, which is noted as Co-P loaded C_3N_4(550).

2.2. Characterization method

Powder XRD was carried out on an X-ray diffractometer (Rint 2000, Altima III, Rigaku Co. Japan) with a Cu Kα source. The morphologies were investigated by scanning electron microscopy (SEM, S4800, Hitachi Co., Japan). The UV–vis absorption was measured with a UV–vis spectrophotometer (Shimadzu, UV-2600) using $BaSO_4$ as the reflectance standard reference. Semi in-situ UV–vis absorption was carried out in Ar by immersing sample with TEOA. After irradiation, the optical absorption spectra were recorded in the diffuse reflectance mode.

XPS measurement was carried out with electron spectrometer (PHI Quantera SXM, ULVAC-PHI Inc., Japan). PL spectra were recorded by a JASCO FP-6500 spectrofluorometer. The fluorescence decay curve was measured using a fluorescent spectrophotometer (Horiba Jobin Yvon, Fluorolog-3) with a nano-LED lamp, excited at 370 nm. ESR measurements were carried out at room temperature on a JEOL JES-FA-200 with the samples adsorbed with TEOA. Solid state 13C MAS NMR was measured on an Infinity plus 300WB spectrometer. FT-IR spectra were recorded by Nicolet 4700 spectrometer. The samples were prepared by mixing the sample with FT-IR-grade KBr (Sigma-Aldrich). FT-IR-grade KBr was used as the reference. All the spectra were collected under nitrogen atmosphere. The Mott-Schottky analysis was conducted in a quartzose beaker and an electrochemical station (ALS-CH model 650A) using three-electrode mode with a platinum foil as the counter electrode and an Ag/AgCl electrode as the reference electrode in 0.2 M Na_2SO_4 aqueous solution. The working electrode was prepared by spin coating a homogeneous turbid liquid composed of 10 mg of sample, 20 μL of 5 wt% Nafion solution and 2 mL ethanol. The Mott-Schottky plots were obtained under direct potential polarization at three different frequencies of 200, 500 and 1000 Hz.

2.3. Photocatalytic experiments

The photocatalytic performance evaluation was carried out on our gaseous photocatalytic system [14]. The sample was dispersed in porous glass fiber uniformly. 1 mL of TEOA (Triethanolamine) and 4 mL of MeCN were mixed and injected into the cell. 80 kPa of pure CO_2 gas was injected into the system after evacuating the reaction system completely. The light source is a 300 W xenon arc lamp with a UV-cut filter and an IR-cut filter to keep the wavelength between 400 nm to 800 nm. The gas products were measured by gas chromatography (GC-14B, Shimadzu Co., Japan). The isotope test using ^{13}C was carried out using gas chromatography-mass spectrometry (JEOL-GCQMS, JMS-K9 and 6890N Network GC system, Agilent Technologies). Wavelength-dependent performance was conducted by using a series of band-pass filters (Optical Coating Japan). The AQE at 420 nm was calculated by the following equation: AQE = (2 × amount of CO molecules evolved in unit time/number of incident photons in unit time) × 100%. The selectivity of CO_2 reduction into CO was calculated by the fol-

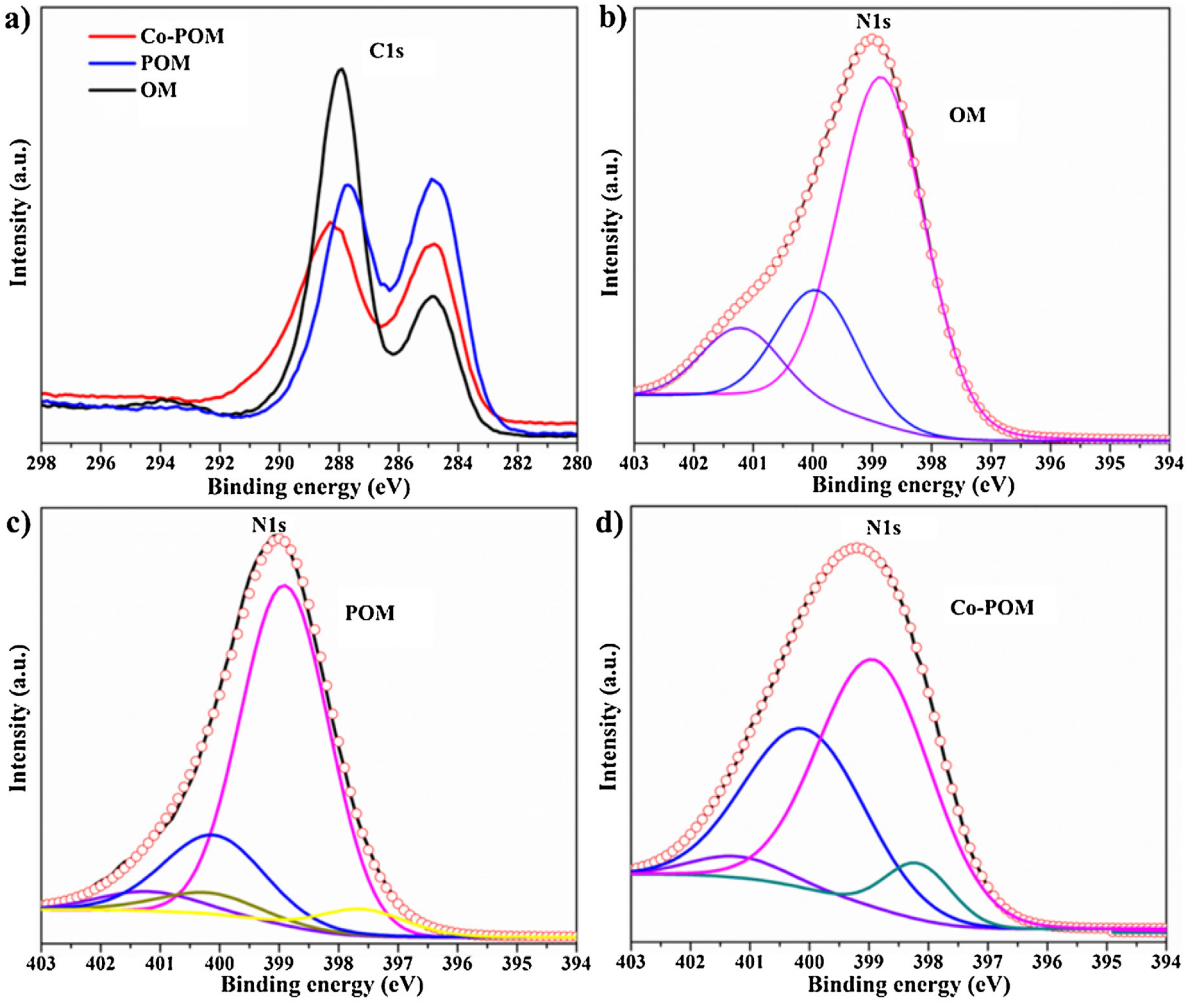

Fig. 3. (a) C 1 s high resolution XPS spectra of OM, POM and Co-POM; Deconvoluted N 1 s spectra for OM (b), POM (c) and Co-POM (d).

lowing equation: Selectivity(CO) = (2 × amount of CO molecules evolved in unit time)/(2 × amount of CO molecules evolved in unit time + 8 × amount of CH_4 molecules evolved in unit time) × 100%.

3. Results and discussion

3.1. Characterization

XRD patterns of POM and Co-POM (Fig. 1a) are similar to that of as synthesized OM, which were difficult to be indexed to one specific space group, indicating the disordered aggregation of these hybrids. SEM images (Fig. S1) of the OM, POM and Co-POM showed a similar block morphology with a lateral dimension in the micrometer scale due to the aggregation.

In the Fourier Transform Infrared Spectroscopy (FTIR) (Fig. 1b), bands at 3490 cm^{-1} and 3420 cm^{-1} can be attributed to the primary amine group on the surface of OM [23,24], which are decreased in intensity for POM and Co-POM after the amino-ketonic condensation. The C=O stretching at 1660 cm^{-1} in the spectra of porphyrin confirmed the successful oxidization of hematoporphyrin in the Jone's reaction. A small spike at 420 cm^{-1} is present in the spectra of Co-POM, indicating the successful Co—N coordination [25]. Unfortunately, the feature stretching vibration of imine linkages at around 1600 cm^{-1} can't be distinguished from the similar signal of heptazine units at 1619 cm^{-1} [26,27]. X-ray photoelectron spectroscopy (XPS) spectrum of Co-POM show a Co $2P_{3/2}$ peak at 780.9 eV, which is characteristic for Co—N chelating, while it is absence in that of OM and POM (Fig. 1c) [28]. In order to confirm that the cobalt is only coordinated with porphyrin units in the hybrid, control experiment was done by refluxing OM with $CoCl_2$ in the same reaction condition and washing with water. XPS of the resulted sample showed no cobalt exists in the carbon nitride (Fig. S2).The TEM image and corresponding Energy Dispersive Spectrometer (EDS) Mapping shown in Fig. 2 also reveal the co-existence and the homogeneous distribution of C, N and Co elements. As detected by ICP-OES, the mass ratios of Co in Co-POM(0.6) and Co-POM are 3.3% and 4.4% respectively, which also reflect the equivalent mole amount of cobalt to porphyrin. The C1s XPS spectra of OM, POM and Co-POM (Fig. 3a) are similar and only different in the intensity ratio of peaks located at 285 eV and 287 eV, which indicate more sp^2 hybridized C—C bonds in POM and Co-POM attributed to the planted porphyrin units. The high-resolution N1s spectra of OM (Fig. 3b) can be assigned to three signals which correspond to pyridinic N (C=N—C, 398.8 eV), tertiary nitrogen (N—C_3, 400.1 eV) and hydrogen-bonded N (NH_2/NH, 401.2 eV) [29,30]. For POM (Fig. 3c), additional signals at 400.2 eV and 397.6 eV were ascribed to the kinds of N in the porphyrin rings, both of which are replaced by a peak at 398.4 eV from Co—N in Co-POM (Fig. 3d) [28]. From thermogravimetric analysis (TGA) in Fig. 1d, it is shown that for pure porphyrin, the pyrolysis occurred at 278 °C, while in POM and Co-POM, the pyrolysis temperature is higher (c.a. 300 °C) than that of porphyrin but lower than that of OM, suggesting that in POM or

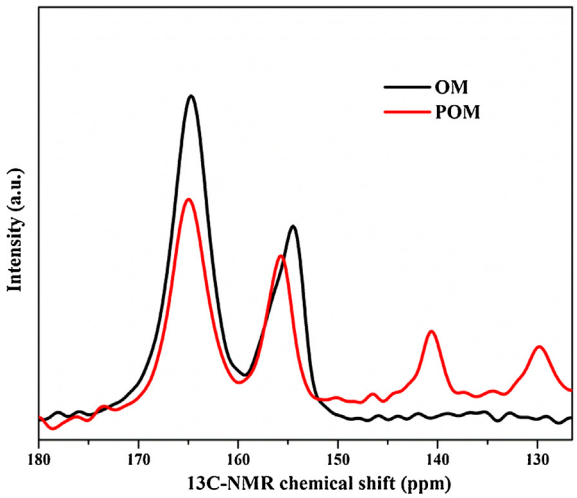

Fig. 4. Solid state ^{13}C NMR spectra of OM and POM.

Co-POM, porphyrin unit or Co-porphyrin unit is not independent with OM.

Solid state ^{13}C NMR spectrum (Fig. 4) exhibits two typical signals of OM, one at 164.6 ppm for the CN_2(NHx) groups and the other at 154.4 ppm for the CN_3 groups [31]. In contrast, the POM contains one signal at higher chemical shift (155.7 ppm), which can be considered as the superimposition signal of imine and CN_3 [32]. The existence of porphyrin units is also confirmed by the featured signal at 140 ppm and 129 ppm [19]. To reconfirm that the porphyrin is not adsorbed on the surface of OM in POM(0.6) and POM, adsorption batch experiment is conducted in the similar condition without adding catalyst for the condensation reaction. The adsorption isotherm (Fig. S3) shows that the maximum adsorption amount of porphyrin towards OM is about 21.74 mg/g, far lower than the reacted amount in POM(0.6) and POM, reflecting that the porphyrin is indeed covalently planted with OM. Combining with the XPS results mentioned above, reaction center/antenna hybrids composed of Co-porphyrin and oligomer of melem was successfully synthesized.

The UV–vis absorption spectra of OM, porphyrin, POM and a physically mixed sample of OM and porphyrin were compared in Fig. 5a. Porphyrin exhibits a broad Soret absorption at about 400 nm and weak Q-bands between 500 and 700 nm [33]. The controlled sample, which is prepared by mixing OM and porphyrin in a small amount of water, and grinding until dried fully, exhibits only the superimposition of OM and porphyrin, while POM shows an inconsistently sloped adsorption edge, which reflects some orbital interaction between OM and porphyrin. Compared with POM, POM(0.6) with less porphyrin subunit showed a similar but lower adsorption, while POM(1.1), due to the higher initial ratio of porphyrin, exhibits consistently sloped adsorption edge, which may be originated from the excessive porphyrin not reacted on the surface. Thus, the maximum covalent loading mass ratio of porphyrin to OM is less than 1.1. Compared with POM(0.6) and POM, Co-POM(0.6) and Co-POM showed a similar but higher optical absorption towards visible light (Fig. 5b).

The red-shift of absorption edge of POM and Co-POM compared with that of OM agrees with the bandgap narrowing as indicated by the transformed Kubelka-Munk function versus the light energy (Fig. 6a). The band gaps and band edges (analyzed from Mott-Schottky measurements in Fig. 6b–d) were listed in Table 1. It is shown that the conduction bands of POM and Co-POM are less negative than that of OM due to the covalent planting of porphyrin unit.

From the results of element analysis, the calculated atomic ratio of C:N:H in OM is about 19.1:29.2:14.9, which is close to that of the ideal trimer heptazine. It is calculated that the average molar ratio of OM to porphyrin unit in POM is about 0.96 according to the mass ratio of OM to porphyrin. It can be deduced that the amine group amount in OM is larger than the loaded porphyrin maximum, which implied that considerable amount of amine group is not reacted with porphyrin. This can be explained by the fact that heterogeneous ketone-amine condensation is not fully efficient and the amount of the exposed surface amine groups is limited due to the severe self-aggregation of OM as shown in the SEM results (Fig. S1).

According to the N_2 adsorption isotherm measurement at 77 K from 0 to 1 atm, the BET surface areas of OM, POM and Co-POM are 3.4, 8.3 and 16.1 m^2/g, respectively (Fig. S4a), which is in agreement with the bulk morphologies. CO_2-adsorption behavior at room temperature (Fig. S4b) indicated that the maximum CO_2 uptake for the three samples was 0.85, 1.27 and 6.74 cm^3/g, respectively. Noting that the BET surface area of Co-POM is only twice that of POM, while CO_2 uptake of Co-POM is about five times that of POM, it is obviously implied that Co-porphyrin site has more affinity towards CO_2 molecule, as confirmed by other reports [34,35].

3.2. Photocatalytic CO_2 reduction

The photocatalytic reduction of CO_2 was conducted in the presence of TEOA as sacrificial agent under visible light with wavelength of 420–800 nm. As shown in Fig. 7a, compared with OM and POM, Co-POM shows significantly enhanced activity. The produced CO is stably increased with a rate of 17 μmol/g/h, and no noticeable change was observed during the four cycling tests (Fig. 7b), while the CH_4 production rate is as low as 0.7 μmol/g/h (not shown here). The calculated selectivity of CO production is around 80%. Control experiments show that light-irradiation, catalyst, TEOA are indispensable for CO_2 conversion. To further confirm the source of CO, pure Ar without CO_2 was used as reactant in a similar photocatalytic condition. Only 0.05 μmol of CO was obtained even after 11 h-irradiation. An isotopic experiment utilizing $^{13}CO_2$ as carbon source was performed in the photocatalytic reaction and the products turned out to be ^{13}CO confirmed by gas chromatography and mass spectra (Fig. S5). All these results indicated that Co-POM was capable of efficiently converting CO_2 into CO under visible light.

It is also shown that Co-POM(0.6) (with lower Co-porphyrin content) had lower activity of 10 μmol/g/h, and both OM and Co-porphyrin (CoP) exhibit limited activity (0.7 μmol/g/h and 3 μmol/g/h, respectively). As inspired by Kuriki et al.'s work [18], Co-porphyrin was mixed with OM in the same ratio as that in Co-POM. The resulted Co-porphyrin loaded C_3N_4 showed a CO evolution rate of 7.2 μmol/g/h, which is higher than pure C_3N_4 without Co-porphyrin (1.4 μmol/g/h) (Fig. 7c). Remarkably, Co-POM showed significant improvement compared with the simply mixed Co-porphyrin/C_3N_4 heterogeneous system. Wavelength dependence of CO evolution (Fig. 7d) revealed that the activity tracked the characteristic optical absorption of Co-POM, suggesting that the CO production is primarily induced by the photo-induced electrons. The calculated apparent quantum efficiency is 0.8% under irradiation at 420 nm. Although the value is quite low compared with the homogeneous CO_2 photocatalytic system using rhenium complex [36], it is still of great importance to the gas-phase CO_2 photoreduction research in consideration of using earth-abundant elements. We also prepared carbon nitride with higher degree of polymerization by heat treatment of melamine at 480 °C (480-OM), which further underwent the condensation with porphyrin and further metallization with $CoCl_2$. As shown in Fig. S6, the resulted 480-POM and 480-Co-POM showed lower increase in optical absorbance toward visible light than POM and Co-POM, sug-

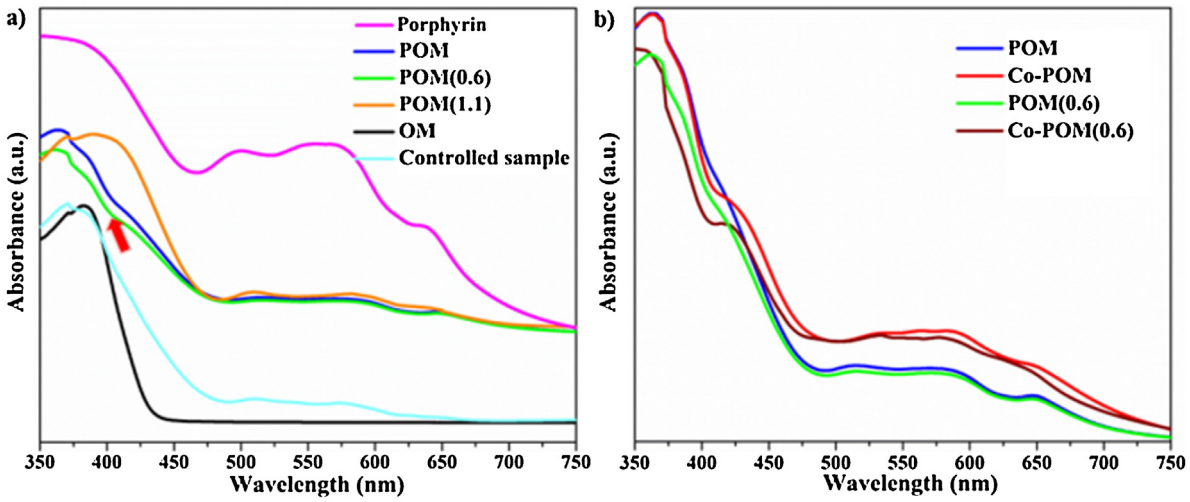

Fig. 5. (a) UV–vis absorption of POM, POM(0.6), POM(1.1), porphyrin, OM and the controlled sample; (b) UV–vis absorption of POM, POM(0.6), Co-POM and Co-POM(0.6) Note: POM, POM(0.6), POM(1.1) were prepared with different mass ratios of OM and porphyrin, i.e., 1:1, 1:0.6 and 1:1.1, respectively; Co-POM and Co-POM(0.6) were derived from the metallization of POM and POM(0.6).

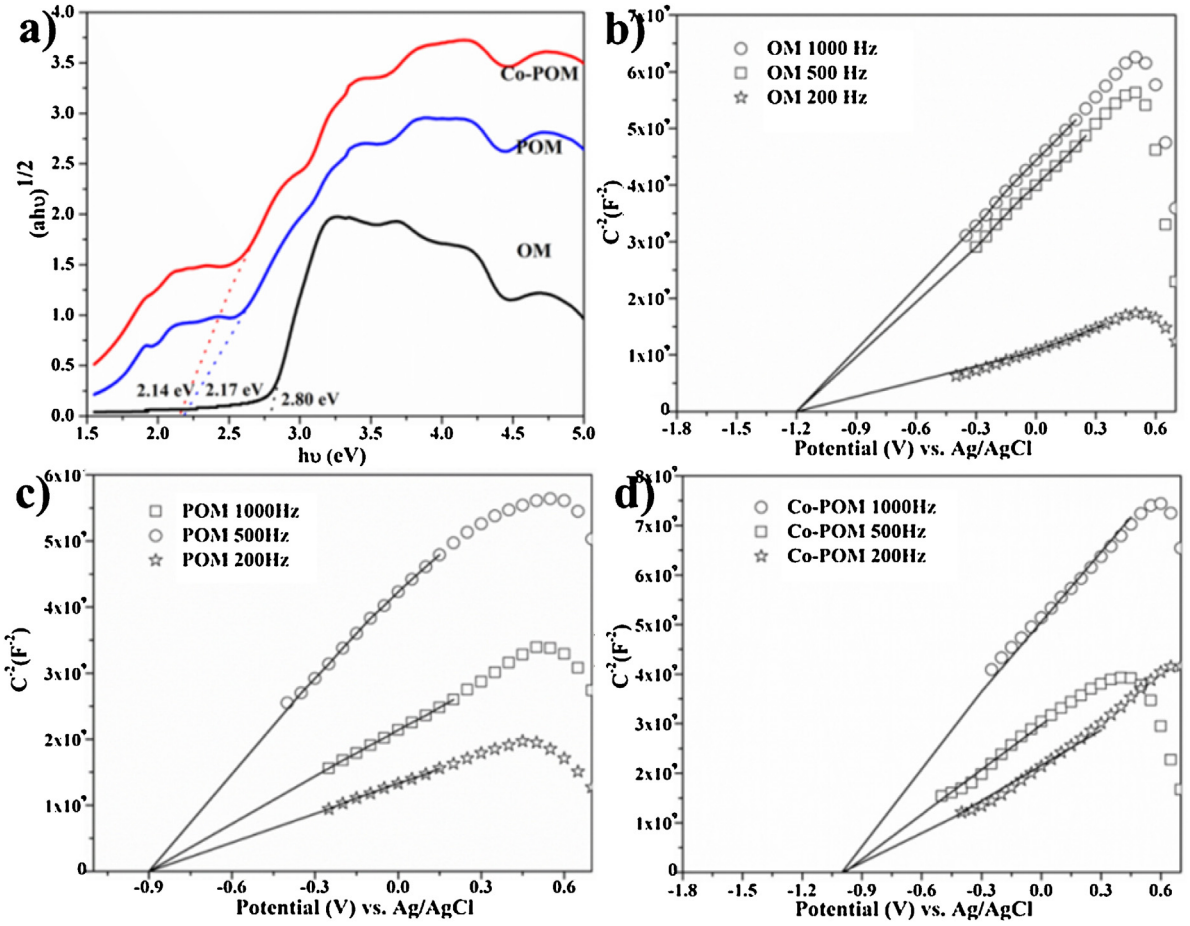

Fig. 6. (a) Plot of Kubelka-Munk function vs. exciting light energy; (b–d) Mott-Schottky plots for OM POM and Co-POM in 0.2 M Na_2SO_4 electrolyte.

Table 1
Comparison of the physical properties of OM, POM and Co-POM.

Sample	Band gap (eV vs. NHE)	Conduction band (eV vs. NHE)	Valence band (eV vs. NHE)	BET surface area (m^2/g)	CO_2 uptake (cm^3/g)
OM	2.80	−0.98	1.82	3.4	0.85
POM	2.17	−0.68	1.49	8.3	1.27
Co-POM	2.14	−0.78	1.36	16.1	6.74

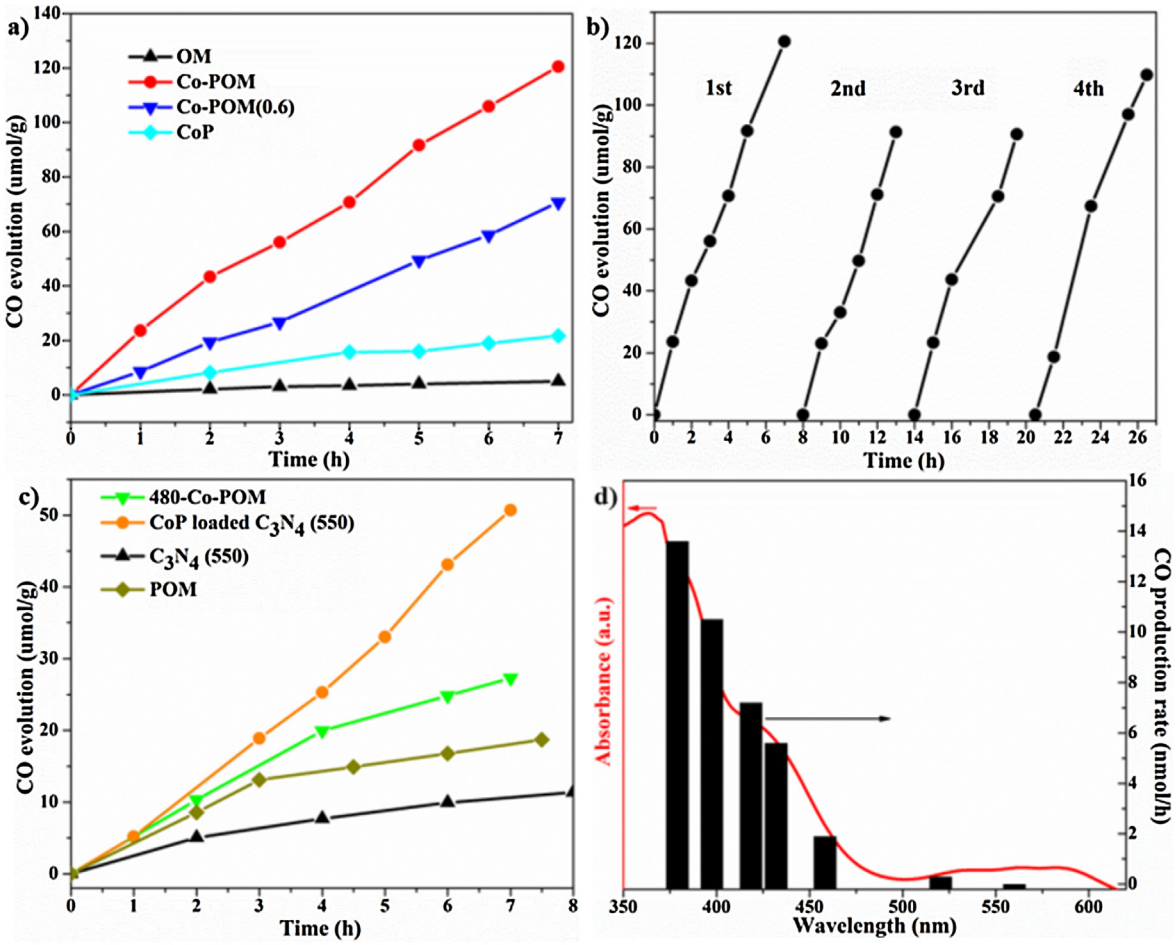

Fig. 7. (a) Time course of CO evolution over OM, Co-POM, Co-POM(0.6) and CoP; (b) Cycling test of the CO evolution over Co-POM; (c) Time course of CO evolution over POM, C_3N_4 (550), CoP loaded C_3N_4 (550) and 480-Co-POM; (d) Wave-length dependence of CO evolution rate over Co-POM. All the samples used are 50 mg and irradiated by 300 W Xe-lamp with a UV-cut filter and an IR-cut filter to keep the wavelength between 400 nm and 800 nm.

gesting a lower amount of planted porphyrin and cobalt, which is further proved by ICP-OES analysis (about 2.6% in mass). The lower Co-porphyrin unit in 480-Co-POM is in agreement with the limited amount of the surface NH_2 group in 480-OM. Under visible light, the CO evolution rate of 480-Co-POM is only about 4 μmol/g/h (Fig. 7c). It is concluded that in such hybrids system, the host carbon nitride is critical to optimize the performance.

It is also noted that compared with OM, POM indeed showed a little higher activity, which should be attributed to the enhanced light-absorption of POM after implanted with porphyrin. However, Co-POM showed a much improved activity relative to POM even the light-absorption of Co-POM is only slightly higher than that of POM. These comparisons indicated that the active Co-site is the crucial factor for the improved CO_2 reduction.

It is necessary to compare the activity with Co ion-incorporated carbon nitride. We have added the preparation of Co-doped C_3N_4 according to the literature [37]. The activity has been evaluated under the same condition. As shown in Fig. S7 (Supplementary Material), the CO evolution rate is about 4.1 μmol/g/h. It is obvious that the implantation of Co-porphyrin is much more beneficial to the CO_2 reduction compared with Co dispersion in carbon nitride.

3.3. Clarification of mechanism

In attempt to understand the mechanism underlying the photocatalytic performance of this covalent hybrid, electron spin resonance (ESR) measurement was carried out with and without irradiation in the presence of TEOA. It can be seen in Fig. 8a, without irradiation, a broad resonance at g = 1.9763 is featured for many Co-porphyrin complexes with D4h symmetry [38], while under visible-light irradiation, such broad signal obviously decreased which may be due to the formation of a low-spin, ESR-silent Co(I) species [39]. For OM, the small signal (g = 2.003) from the aromatic heptazine structure under irradiation showed no enhanced intensity compared with that in dark, which may be due to its low optical absorption in visible light [14]. The accumulation of Co(I) in the presence of TEOA is also monitored by semi-in situ UV–vis spectroscopy (Fig. 8b). Once irradiated, a broad absorption band at 550–570 nm emerged and the intensity increased with irradiation time, which is considered as a characteristic of Co(I) porphyrin [19,40] and other Co(I) species with similar Co—N coordination structure [41,42]. From the photoluminescence (PL) measurements for OM, POM and Co-POM by exciting at 390 nm shown in Fig. 8c, OM showed strong PL at 440 nm. After planting with porphyrin, POM showed a PL emission quenching centered at 485 nm, which is in agreement with the red-shift optical absorption in Fig. 5a. Although in the absorption spectra, POM and Co-POM showed similar optical-absorption edge with onset near 2.6 eV, Co-POM exhibits a 15 nm red-shift PL relative to POM, which implied that there existed some intermediate energy level related with the Co. The fluorescence-lifetime measurement (Fig. 8d) revealed that the average lifetime for Co-POM (monitored at 500 nm) is about 698 ns, much longer than those for POM (174 ns, monitored at 485 nm) and OM (91.7 ns, monitored at 440 nm), which fully implied that

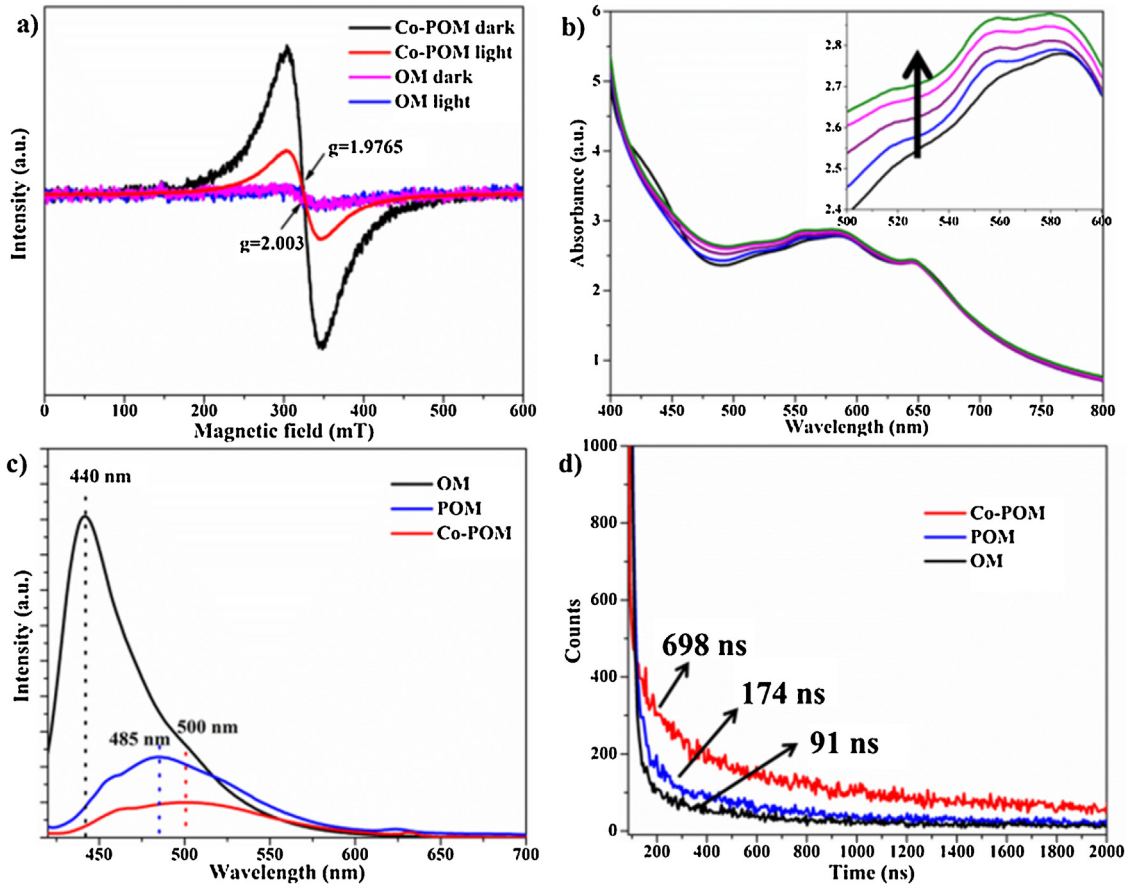

Fig. 8. (a) ESR spectra of Co-POM and OM under irradiation and dark condition; (b) Semi-in situ UV–vis absorption spectra changes recorded over Co-POM immersed in TEOA protected in Ar at room temperature during the irradiation under visible light (irradiation time 0–4 min, 1 min intervals). Inset is the enlarged view; (c) PL spectra and (d) decay curve of OM, POM and Co-POM, PL recorded with excitation at 350 nm and decay curve were monitored at 440 nm, 485 nm and 500 nm, respectively.

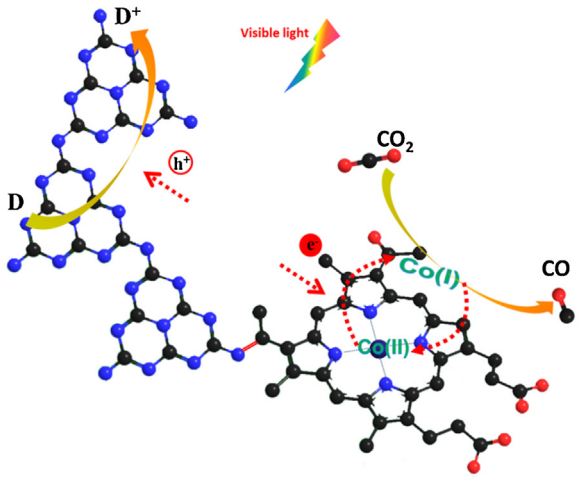

Fig. 9. Possible mechanism of CO_2 reduction over Co-POM under visible light.

the activated state in Co-POM is longer-lived than that in POM and OM.

By combining the discussed ESR and Semi-in situ UV–vis absorption results, we inferred that in the Co-POM hybrids, the interaction between heptazine-porphyrin network and Co(II) could induce a more delocalized Co(II) electronic structure, similar to the case of the COF comprising Co-porphyrin [19]. As illustrated in Fig. 9, with irradiation, the photogenerated electron-hole could be separated more efficiently in the covalent bridged hybrids since electrons could be easily trapped by Co(II) to form Co(I) species, which is supposed energetically located closely to the conduction band of Co-POM [43]. When CO_2 happened to bind with Co-porphyrin site, CO_2 reduction can be occurred to form CO in a path illustrated by many previous researches [44,45].

4. Conclusions

In summary, we have fabricated a reaction center/antenna hybrids based on Co-porphyrin and carbon nitride by a judicious condensation of low oligomeric carbon nitride and porphyrin and the following metallization of porphyrin ring. The resulted Co-POM hybrids showed higher CO_2 affinity, improved electron-hole separation and prolonged lifetime of the excited state due to the internal electron trap by Co(II) sites, which contributed to the enhanced photocatalytic CO_2 reduction activity (17 μmol/g/h) compared with that of bulk C_3N_4 (1.4 μmol/g/h) and Co-porphyrin loaded C_3N_4 (7.2 μmol/g/h). More importantly, the covalent combination of light harvest antenna and active sites has been demonstrated to play a great role in promoting photocatalytic activity, which would inspire more ingenious designing for mimic photosynthesis.

Acknowledgements

This work was partially supported by JSPS (Japan Society for the Promotion of Science) Postdoctoral Fellowship for Foreign Researchers, the World Premier International Research Center Ini-

tiative (WPI Initiative) on Materials Nanoarchitectonics (MANA) (Japan).

Appendix A. Supplementary data

Supplementary data associated with this article can be found, in the online version, at http://dx.doi.org/10.1016/j.apcatb.2016.06.074.

References

[1] W.-H. Wang, Y. Himeda, J.T. Muckerman, G.F. Manbeck, E. Fujita, Chem. Rev. 115 (2015) 12936–12973.
[2] W. Tu, Y. Zhou, Z. Zou, Adv. Mater. 26 (2014) 4607–4626.
[3] H. Tong, S. Ouyang, Y. Bi, N. Umezawa, M. Oshikiri, J. Ye, Adv. Mater. 24 (2012) 229–251.
[4] H. Liu, X. Meng, T.D. Dao, H. Zhang, P. Li, K. Chang, T. Wang, M. Li, T. Nagao, J. Ye, Angew. Chem. Int. Ed. 54 (2015) 11545–11549.
[5] K. Sekizawa, K. Maeda, K. Domen, K. Koike, O. Ishitani, J. Am. Chem. Soc. 135 (2013) 4596–4599.
[6] Q. Kang, T. Wang, P. Li, L. Liu, K. Chang, M. Li, J. Ye, Angew. Chem. Int. Ed. 54 (2015) 841–845.
[7] T. Baran, S. Wojtyła, A. Dibenedetto, M. Aresta, W. Macyk, Appl. Catal. B: Environ. 178 (2015) 170–176.
[8] B. Pan, S. Luo, W. Su, X. Wang, Appl. Catal. B: Environ. 168–169 (2015) 458–464.
[9] M. Wang, D. Wang, Z. Li, Appl. Catal. B: Environ. 183 (2016) 47–52.
[10] X. Wang, K. Maeda, A. Thomas, K. Takanabe, G. Xin, J.M. Carlsson, K. Domen, M. Antonietti, Nat. Mater. 8 (2009) 76–80.
[11] J. Mao, T. Peng, X. Zhang, K. Li, L. Ye, L. Zan, Catal. Sci. Technol. 3 (2013) 1253–1260.
[12] H. Li, S. Gan, H. Wang, D. Han, L. Niu, Adv. Mater. 27 (2015) 6906–6913.
[13] H. Shi, G. Chen, C. Zhang, Z. Zou, ACS Catal. 4 (2014) 3637–3643.
[14] L. Shi, T. Wang, H. Zhang, K. Chang, J. Ye, Adv. Funct. Mater. 25 (2015) 5360–5367.
[15] J. Lin, Z. Pan, X. Wang, ACS Sustain. Chem. Eng. 2 (2014) 353–358.
[16] R. Kuriki, H. Matsunaga, T. Nakashima, K. Wada, A. Yamakata, O. Ishitani, K. Maeda, J. Am. Chem. Soc. 138 (2016) 5159–5170.
[17] K. Maeda, R. Kuriki, M. Zhang, X. Wang, O. Ishitani, J. Mater. Chem. A 2 (2014) 15146–15151.
[18] R. Kuriki, K. Sekizawa, O. Ishitani, K. Maeda, Angew. Chem. Int. Ed. 54 (2015) 2406–2409.
[19] S. Lin, C.S. Diercks, Y.-B. Zhang, N. Kornienko, E.M. Nichols, Y. Zhao, A.R. Paris, D. Kim, P. Yang, O.M. Yaghi, C.J. Chang, Science 349 (2015) 1208–1213.
[20] L. Chen, Z. Guo, X.-G. Wei, C. Gallenkamp, J. Bonin, E. Anxolabéhère-Mallart, K.-C. Lau, T.-C. Lau, M. Robert, J. Am. Chem. Soc. 137 (2015) 10918–10921.
[21] J. Shen, R. Kortlever, R. Kas, Y.Y. Birdja, O. Diaz-Morales, Y. Kwon, I. Ledezma-Yanez, K.J.P. Schouten, G. Mul, M.T.M. Koper, Nat. Commun. 6 (2015) 8177.
[22] A. Maurin, M. Robert, J. Am. Chem. Soc. 138 (2016) 2492–2495.
[23] V.Y. Sosnovskikh, Mendeleev Commun. 6 (1996) 189–190.
[24] B.V. Lotsch, W. Schnick, Chem. Eur. J. 13 (2007) 4956–4968.
[25] J. Haber, M. Kłosowski, J. Połtowicz, J. Mol. Catal. A: Chem. 201 (2003) 167–178.
[26] B.V. Lotsch, M. Döblinger, J. Sehnert, L. Seyfarth, J. Senker, O. Oeckler, W. Schnick, Chem. Eur. J. 13 (2007) 4969–4980.
[27] A. Satake, Y. Miyajima, Y. Kobuke, Chem. Mater. 17 (2005) 716–724.
[28] T. Okada, M. Gokita, M. Yuasa, I. Sekine, J. Electrochem. Soc. 145 (1998) 815–822.
[29] Q. Liu, J. Zhang, Langmuir 29 (2013) 3821–3828.
[30] A. Thomas, A. Fischer, F. Goettmann, M. Antonietti, J.-O. Muller, R. Schlogl, J.M. Carlsson, J. Mater. Chem. 18 (2008) 4893–4908.
[31] B. Jürgens, E. Irran, J. Senker, P. Kroll, H. Müller, W. Schnick, J. Am. Chem. Soc. 125 (2003) 10288–10300.
[32] M.G. Schwab, M. Hamburger, X. Feng, J. Shu, H.W. Spiess, X. Wang, M. Antonietti, K. Mullen, Chem. Commun. 46 (2010) 8932–8934.
[33] Y. Xu, Z. Liu, X. Zhang, Y. Wang, J. Tian, Y. Huang, Y. Ma, X. Zhang, Y. Chen, Adv. Mater. 21 (2009) 1275–1279.
[34] H.S. Choi, H.J. Jeon, J.H. Choi, G.-H. Lee, J.K. Kang, Nanoscale 7 (2015) 18923–18927.
[35] V.S.P.K. Neti, J. Wang, S. Deng, L. Echegoyen, J. Mater. Chem. A 3 (2015) 10284–10288.
[36] H. Takeda, K. Koike, H. Inoue, O. Ishitani, J. Am. Chem. Soc. 130 (2008) 2023–2031.
[37] G. Zhang, C. Huang, X. Wang, Small 11 (2015) 1215–1221.
[38] D.V. Konarev, I.S. Neretin, Y.L. Slovokhotov, E.I. Yudanova, N.y.V. Drichko, Y.M. Shul'ga, B.P. Tarasov, L.L. Gumanov, A.S. Batsanov, J.A.K. Howard, R.N. Lyubovskaya, Chem. Eur. J. 7 (2001) 2605–2616.
[39] J.G. McAlpin, Y. Surendranath, M. Dincă, T.A. Stich, S.A. Stoian, W.H. Casey, D.G. Nocera, R.D. Britt, J. Am. Chem. Soc. 132 (2010) 6882–6883.
[40] D. Behar, T. Dhanasekaran, P. Neta, C.M. Hosten, D. Ejeh, P. Hambright, E. Fujita, J. Phys. Chem. A 102 (1998) 2870–2877.
[41] G. Smolentsev, B. Cecconi, A. Guda, M. Chavarot-Kerlidou, J.A. van Bokhoven, M. Nachtegaal, V. Artero, Chem. Eur. J. 21 (2015) 15158–15162.
[42] D.P. Estes, D.C. Grills, J.R. Norton, J. Am. Chem. Soc. 136 (2014) 17362–17365.
[43] M.-S. Liao, S. Scheiner, J. Chem. Phys. 114 (2001) 9780–9791.
[44] K. Leung, I.M.B. Nielsen, N. Sai, C. Medforth, J.A. Shelnutt, J. Phys. Chem. A 114 (2010) 10174–10184.
[45] I.M.B. Nielsen, K. Leung, J. Phys. Chem. A 114 (2010) 10166–10173.